Angle- and spin-resolved photoemission from ferromagnets

1996 J. Phys.: Condens. Matter 8 4971

(http://iopscience.iop.org/0953-8984/8/27/008)

J. Phys.: Condens. Matter **8** (1996) 4971–4981. Printed in the UK

Angle- and spin-resolved photoemission from ferromagnets

N A Cherepkov†§ and V V Kuznetsov‡

† Universität Bielefeld, Fakultät für Physik, Postfach 100131, 33501 Bielefeld, Germany
‡ State Academy of Aerospace Instrumentation, 190000 St Petersburg, Russia

Received 22 January 1996, in final form 14 March 1996

Abstract. Equations for angle- and spin-resolved photoemission from core levels of ferromagnets are derived using the atomic model. They are applied to the np subshells and to the particular geometries of experiment with the photoemission normal to the surface, which have been used already in several experiments. It is shown that for these geometries the spin-resolved spectra obtained with linearly polarized light are especially simple and contain the contribution of only one or two magnetic sublevels of the $np_{3/2}$ state, and of only one sublevel of the $np_{1/2}$ state, which allow one to resolve the magnetic splitting of core levels. The use of circularly polarized or unpolarized light gives a less transparent picture.

1. Introduction

Recent experimental investigations [1–10] have shown that the shape of photoelectron spectra from the core levels of ferromagnets are essentially changed when the direction of magnetization is reversed. The difference between two spectra obtained with opposite directions of sample magnetizations was called magnetic x-ray dichroism in photoemission [1], or magnetic dichroism in angular distribution (MDAD) of photoelectrons [5]. The effect exists for all kinds of light polarization, namely for circular [1–3], linear [4–7] and even unpolarized [8, 9] light. Spin-resolved measurements also revealed that in each spin channel the shapes of photoelectron spectra are different [4, 10]. From the very beginning [1] it was clear that the observed phenomena appear as a result of the energy splitting of a particular core level due to exchange interaction with the valence-band d (or f) electrons. The first numerical calculations performed for the 2p subshell of Fe in [11] and for the 3d valence band of Ni in [12] fully supported this general conclusion. In recently published theoretical papers [13, 14] the general properties of the angular distributions of photoelectrons emitted from ferromagnets have been discussed, but without a detailed analysis of the experiments already performed and of the kind of information which can be extracted from these experiments. We would like to fill this gap and to present the qualitative analysis of the spin-resolved spectra using the atomic model for the description of the process.

Previously it has already been shown [15] that all the qualitative features of MDAD spectra can be adequately described by the atomic model, but in [15] the spin polarization of electrons was disregarded. Therefore the main purpose of this paper is to extend this model in order to include the photoelectron spin also in our considerations and to describe the general features of the angle- and spin-resolved photoelectron spectra from ferromagnets

§ Permanent address: State Academy of Aerospace Instrumentation, 190000 St Petersburg, Russia.

0953-8984/96/274971+11$19.50

which follow from the atomic model without any numerical calculation. This model should be applicable for the description of photoemission from core levels, when the photoelectron energy is high enough to neglect the scattering processes. A recent investigation of spin polarization in Cu core level photoemission [16] clearly demonstrated that the atomic model can be successfully applied to a quantitative analysis of angle- and spin-resolved photoemission from solids, in that case from non-magnetic solids. The main advantage of using the atomic model is the simplicity of the analytical equations which make it easy both to analyse them qualitatively and to perform numerical calculations with different kinds of approximate wavefunction. Then, from the comparison with experiment, one can make a conclusion on the importance of the solid state effects in the process under consideration. In addition, the general equations obtained in the atomic model enables one to estimate the quality of some rather arbitrary approximations made in model considerations when, for example, the interference terms between $l+1$ and $l-1$ continua are neglected [17].

2. General theory

Consider the photoionization of atoms in the electric-dipole approximation, taking into account only one-electron processes. If in the initial state the ionized subshell is closed, in the final state there will be a hole characterized by the quantum numbers nlj with j being the total angular momentum. Owing to exchange interaction with the open valence shell in ferromagnets, each nlj state will be energetically split into components with a given projection m_j. Thus each sublevel of the hole state will be characterized by the quantum numbers $nljm_j$ and therefore will be polarized. This characterization of the hole states is justified when the spin–orbit splitting is larger than the exchange splitting, as for example in the 2p subshell of Fe. In the 3p subshell of Fe the exchange splitting is nearly as large as the spin–orbit splitting (see [17] and references therein), so that our characterization of the hole states will be less appropriate. We shall not consider explicitly the exchange interaction between the hole state and an open nd or nf subshell, and we shall disregard the total angular momentum of the outer shell because it will not be a good quantum number in solids. This is justified when the bandwidth of conduction electrons is large compared with the magnetic splitting of the core hole state, which corresponds to a high hopping rate of conduction electrons [18]. The latter approximation is used in almost all papers devoted to this problem. So, the ferromagnetic nature of the solid is described in our model by introducing the energy splitting of core hole magnetic sublevels. The magnitude of this splitting does not influence the angular dependence of the spin polarization and therefore can be considered simply as an empirical parameter. This is in full analogy to the fact that the spin polarization of atomic photoelectrons ejected from unpolarized atoms does not depend on the strength of the spin–orbit interaction as soon as the spin–orbit splitting of atomic levels has been resolved [19].

It is easy to show [19] that the photoionization of a closed subshell when the final ionic state is polarized is described by the same equations as the photoionization of a one-electron subshell with the same orbital and total angular momenta which is initially polarized. Therefore for simplicity we shall imply in the derivation below that a one-electron subshell nlj is ionized. Since each magnetic sublevel is populated incoherently, the corresponding atomic density matrix is diagonal in the coordinate frame whose Z axis coincides with the atomic polarization direction $\boldsymbol{n}$. If the direction $\boldsymbol{n}$ does not coincide with the Z axis of our

laboratory frame, we can diagonalize the density matrix by a rotation

$$\langle jm_j|\rho_a|jm'_j\rangle = \sum_{m_1} D^{j}_{m_j m_1}(\Omega)\langle jm_1|\rho^{\boldsymbol{n}}_a|jm_1\rangle D^{j*}_{m'_j m_1}(\Omega). \tag{1}$$

The quantities $D^{j}_{m_j m_1}(\Omega)$ are Wigner rotation matrices [20], and Ω denotes the Euler angles corresponding to the rotation from the laboratory Z axis to the direction $\boldsymbol{n}$ of the atomic polarization. In the following we shall imply that our laboratory frame is defined by the photon beam, so that its Z axis coincides with the direction of the photon beam.

A general expression for the angular distribution of photoelectrons with defined spin polarization ejected from polarized atoms in our laboratory frame is [21–23]

$$\begin{aligned} I_j(\boldsymbol{\kappa}, \boldsymbol{s}, \boldsymbol{n}) = \frac{\alpha\omega p}{2\pi} \sum_{\lambda,\lambda'} \sum_{\mu_1,\mu_2} \sum_{m_j,m'_j} &\langle \Psi^{-}_{\boldsymbol{p}\mu_1}|d_\lambda|\Psi_{nljm_j}\rangle\langle jm_j|\rho_a|jm'_j\rangle \\ &\times\langle\lambda|\rho^{\gamma}|\lambda'\rangle\langle\Psi_{nljm'_j}|d^{*}_{\lambda'}|\Psi^{-}_{\boldsymbol{p}\mu_2}\rangle\langle\mu_2|\tfrac{1}{2}(1+\boldsymbol{s}\cdot\boldsymbol{\sigma})|\mu_1\rangle \end{aligned} \tag{2}$$

where α is the fine-structure constant, ω is the photon energy, $\boldsymbol{p}$ is the photoelectron momentum, $\boldsymbol{\kappa} = \boldsymbol{p}/p$, $\boldsymbol{s}$ is the unit vector in the direction of the photoelectron spin, μ is the projection of spin on the laboratory Z axis, $\boldsymbol{\sigma}$ is the Pauli matrix vector, Ψ_{nljm} is the initial-state wavefunction, $\Psi^{-}_{\boldsymbol{p}\mu}$ is the final-state wavefunction which contains in the asymptotic region the superposition of a plane wave propagating in the direction of the electron momentum $\boldsymbol{p}$ and a converging spherical wave, and ρ^{γ} is the photon density matrix. Neglecting spin–orbit interaction in continuous spectrum, we obtain the following equation for the dipole matrix elements in (2) [24]:

$$\begin{aligned} \langle\Psi^{-}_{\boldsymbol{p}\mu}|d_\lambda|\Psi_{nljm_j}\rangle = \frac{2\pi}{\sqrt{p}} \sum_{l_1,m_1} \sum_{m} &[j]^{1/2}(-\mathrm{i})^{l_1}\exp(\mathrm{i}\delta_{l_1})Y_{l_1 m_1}(\hat{\boldsymbol{\kappa}})(-1)^{1/2-l-m_j+l_1-m_1} \\ &\times \begin{pmatrix} l & \frac{1}{2} & j \\ m & \mu & -m_j \end{pmatrix} \begin{pmatrix} l_1 & 1 & l \\ -m_1 & \lambda & m \end{pmatrix} \langle\varepsilon l_1\|d\|nlj\rangle. \end{aligned} \tag{3}$$

Here δ_{l_1} is the partial-wave phase shift and $\langle\varepsilon l_1\|d\|nlj\rangle$ is the reduced dipole matrix element.

Instead of density matrices it is more convenient in our derivation to use the state multipoles. The photon density matrix in the laboratory frame can be expanded in state multipoles according to the equation [25]

$$\langle\lambda|\rho^{\gamma}|\lambda'\rangle = \sum_{k,\kappa}(-1)^{1-\lambda}[k]^{1/2} \begin{pmatrix} 1 & 1 & k \\ \lambda & -\lambda' & -\kappa \end{pmatrix} \rho^{\gamma}_{k\kappa} \tag{4}$$

where $[k] \equiv (2k+1)$ and the state multipoles $\rho^{\gamma}_{k\kappa}$ can be expressed through the Stokes parameters. The atomic density matrix in (2) should be at first transformed into the coordinate frame where it is diagonal according to (1) and then expanded in state multipoles similar to (4). Then in the laboratory frame we obtain finally

$$\langle jm_j|\rho_a|jm'_j\rangle = \sum_{N,M_N} \sqrt{4\pi}(-1)^{j-m_j} \begin{pmatrix} j & j & N \\ m_j & -m'_j & -M_N \end{pmatrix} Y^{*}_{NM_N}(\hat{\boldsymbol{n}})\rho^{\boldsymbol{n}}_{N0}. \tag{5}$$

Here only the state multipoles $\rho^{\boldsymbol{n}}_{N0}$ with zero projections remain. Finally, the spin projection operator in (2) can be presented as follows:

$$\langle\mu_2|\tfrac{1}{2}(1+\boldsymbol{s}\cdot\boldsymbol{\sigma})|\mu_1\rangle = \sqrt{2\pi}\sum_{x,\xi}(-1)^{1/2-\mu_2} \begin{pmatrix} \frac{1}{2} & \frac{1}{2} & x \\ \mu_2 & -\mu_1 & -\xi \end{pmatrix} Y^{*}_{x\xi}(\hat{\boldsymbol{s}}). \tag{6}$$

Substituting the definitions (3)–(6), and performing summations over projections of angular momenta, we find that [26]

$$I_j(\boldsymbol{\kappa}, \boldsymbol{s}, \boldsymbol{n}) = \sigma_{nlj}(\omega)\sqrt{6\pi[l]}\sum_{k,\kappa}\sum_{x,\xi}\sum_{L,M}\sum_{N,M_N}\sum_{y,\eta}[j, y][k, L]^{1/2}(-1)^{N-\eta}Z_{kLy}\rho^{\gamma}_{k\kappa}\rho^{n}_{N0}$$
$$\times\begin{pmatrix} x & y & N \\ -\xi & \eta & -M_N \end{pmatrix}\begin{pmatrix} k & L & y \\ \kappa & M & \eta \end{pmatrix}\begin{Bmatrix} y & N & x \\ l & j & \frac{1}{2} \\ l & j & \frac{1}{2} \end{Bmatrix} Y^*_{LM}(\hat{\boldsymbol{\kappa}})Y^*_{x\xi}(\hat{\boldsymbol{s}})Y^*_{NM_N}(\hat{\boldsymbol{n}}) \tag{7}$$

where

$$Z_{kLy} = \sqrt{3[l]}B^{-1}\sum_{l_1,l_2}(\mathrm{i})^{l_1-l_2}\exp[\mathrm{i}(\delta_{l_1}-\delta_{l_2})][l_1, l_2]^{1/2}(-1)^{l_2}\begin{pmatrix} l_1 & l_2 & L \\ 0 & 0 & 0 \end{pmatrix}\begin{Bmatrix} k & L & y \\ 1 & l_2 & l \\ 1 & l_1 & l \end{Bmatrix}$$
$$\times\langle\varepsilon l_1\|d\|nlj\rangle\langle nlj\|d\|\varepsilon l_2\rangle \tag{8}$$

$$B = \sum_{l_1}|\langle\varepsilon l_1\|d\|nlj\rangle|^2 \tag{9}$$

and the photoionization cross section is

$$\sigma_{nlj}(\omega) = \frac{4\pi^2\alpha\omega B}{3[l]}. \tag{10}$$

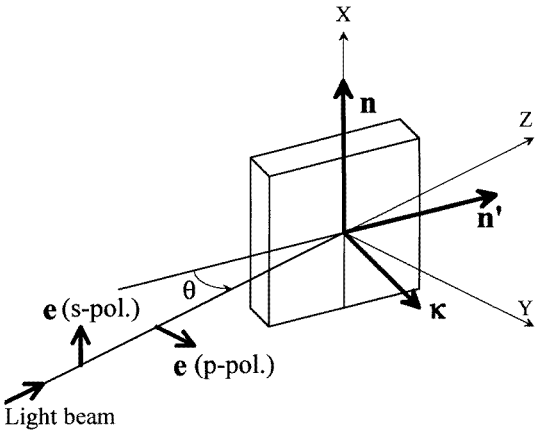

Figure 1. Definition of the geometry of the experiments.

If the spin–orbit interaction in the continuous spectrum is taken into account, equation (8) will change, while equation (7) remains valid. Therefore the latter can be used for a general analysis of the angular distributions. Up to now nobody has analysed the general equation (7) in application to free polarized atoms because in that case it is sufficient to find out the angular distribution without determining the spin polarization in order to obtain the complete characterization of the process [23].

In the general case of arbitrary directions of all three vectors $\boldsymbol{\kappa}$, $\boldsymbol{s}$ and $\boldsymbol{n}$ there are too many terms in the angular distribution (7) in order to write them explicitly, as was done in the case of the spin-integrated angular distribution in [27]. However, for particular geometries of the experiment when some of the vectors are parallel or perpendicular to each

other, the number of terms in (7) can be essentially reduced, which makes the analysis of the angular distribution feasible.

3. Particular geometries of experiment

In this section we shall apply the general equation (7) to the particular cases of photoemission from np subshells considered in several experiments. Figure 1 shows the geometry of experiment used in [4] for an angle- and spin-resolved photoemission study from the 3p core level of magnetized Fe with linearly polarized light. In this experiment $\boldsymbol{s}$ and $\boldsymbol{n}$ are either parallel or antiparallel to each other and are perpendicular to the light beam, photoelectrons are detected in the direction of the surface normal so that $\boldsymbol{\kappa} \perp \boldsymbol{n}$ and $\boldsymbol{\kappa} \perp \boldsymbol{s}$, and the light is linearly polarized perpendicular to the direction of magnetization. From equation (7) we obtain the following expressions for $n\mathrm{p}_{1/2}$ and $n\mathrm{p}_{3/2}$ hole states:

$$I_{1/2}(\boldsymbol{\kappa}, \boldsymbol{s}, \boldsymbol{n}) = \frac{\sigma(\omega)}{4\pi\sqrt{2}}(\rho_{00}^{n} \mp \rho_{10}^{n})[1 + \beta - \tfrac{3}{2}\beta \sin^2\theta \pm \eta^{1/2}\sin(2\theta)] \tag{11}$$

$$I_{3/2}(\boldsymbol{\kappa}, \boldsymbol{s}, \boldsymbol{n}) = \frac{\sigma(\omega)}{4\pi}\left[\left(\rho_{00}^{n} + \tfrac{1}{2}\rho_{20}^{n} \pm \frac{2}{\sqrt{5}}\rho_{10}^{n} \pm \frac{3}{2\sqrt{5}}\rho_{30}^{n}\right) \times (1 + \beta - \tfrac{3}{2}\beta\sin^2\theta) \pm (\rho_{00}^{n} + 2\rho_{20}^{n} \pm \sqrt{5}\rho_{10}^{n})\eta^{3/2}\sin(2\theta)\right] \tag{12}$$

where β is the usual angular asymmetry parameter, η^{j} is the spin polarization parameter defined by equation (14) of [24], and the upper and lower signs refer to $\boldsymbol{s} \| \boldsymbol{n}$ and $\boldsymbol{s} \| -\boldsymbol{n}$, which we shall denote in the following as $(M\uparrow, s\uparrow)$ (magnetization up, spin up) and $(M\uparrow, s\downarrow)$ (magnetization up, spin down). The equations for $(M\downarrow, s\downarrow)$ and $(M\downarrow, s\uparrow)$ differ from the corresponding equations (11) and (12) for $(M\uparrow, s\uparrow)$ and $(M\uparrow, s\downarrow)$ by the change in sign of the term with $\sin(2\theta)$. It is worth while to note that equations (11) and (12) contain the contribution of ρ_{30}^{n} which was absent in MDAD for the same geometry of experiment [15].

Using the state multipoles which for all magnetic sublevels of the $n\mathrm{p}_{3/2}$ and $n\mathrm{p}_{1/2}$ states are given in table 1, one can easily find that for some magnetic sublevels the linear combinations of state multipoles in (11) and (12) turn out to be equal to zero. In other words, not all magnetic sublevels contribute to the photoelectron current. This conclusion does not depend on whether the spin–orbit interaction in the continuous spectrum is taken into account or not. Table 2 shows explicitly the relative contribution of each magnetic sublevel to the photoelectron current for the geometry of experiment under consideration. Unity in this table means that the intensity of a given sublevel in the spin-resolved spectrum is the same as in the spin-unresolved spectrum. If the spin-unresolved spectrum for a given magnetization is fitted by Lorentzian peaks, then the spin-resolved spectrum is obtained from it by multiplying the fitted intensities by the coefficients given in table 2. This procedure has already been used in [7] to simulate the spin-resolved spectra. It is seen from table 2 that only two magnetic sublevels of the $n\mathrm{p}_{3/2}$ core level and one magnetic sublevel of the $n\mathrm{p}_{1/2}$ level contribute to the spin-resolved spectra. Therefore the photoelectron spectrum from the $n\mathrm{p}_{1/2}$ subshell should have a single-peak structure for both magnetizations with the peak position in the magnetization-down spectrum shifted towards lower binding energies, while in the $n\mathrm{p}_{3/2}$ spectrum there should be a double-peak structure for both magnetization directions, and these two peaks for the magnetization-up spectrum should be shifted towards the lower binding energies compared with the magnetization-down spectrum. This is in

accord with the only published experimental observation (see figure 3 in [4]) where double-peak structures have been observed in the region of $3p_{3/2}$ photoemission from Fe (the $3p_{1/2}$ contribution could not be clearly separated in these data). It is also seen that the positions of two peaks on both curves in the lower part of this figure which corresponds to $\boldsymbol{s}\|\boldsymbol{n}$ are shifted to lower binding energies compared with the two peaks on both curves in the upper part of this figure which corresponds to $\boldsymbol{s}\|-\boldsymbol{n}$, again in accord with the results in table 2. The problem of determining the contribution of $3p_{1/2}$ level still remains, and it is discussed in more detail in [28]. Analysis of new experimental data for the 2p subshell of Fe using the atomic model will be given elsewhere [29].

Table 1. State multipoles $\rho^{\boldsymbol{n}}_{N0}$ for magnetic sublevels of $np_{1/2}$ and $np_{3/2}$ states.

j	m_j	$\rho^{\boldsymbol{n}}_{00}$	$\rho^{\boldsymbol{n}}_{10}$	$\rho^{\boldsymbol{n}}_{20}$	$\rho^{\boldsymbol{n}}_{30}$
$\frac{1}{2}$	$\frac{1}{2}$	$\frac{1}{\sqrt{2}}$	$\frac{1}{\sqrt{2}}$	0	0
$\frac{1}{2}$	$-\frac{1}{2}$	$\frac{1}{\sqrt{2}}$	$-\frac{1}{\sqrt{2}}$	0	0
$\frac{3}{2}$	$\frac{3}{2}$	$\frac{1}{2}$	$\frac{3}{2\sqrt{5}}$	$\frac{1}{2}$	$\frac{1}{2\sqrt{5}}$
$\frac{3}{2}$	$\frac{1}{2}$	$\frac{1}{2}$	$\frac{1}{2\sqrt{5}}$	$-\frac{1}{2}$	$-\frac{3}{2\sqrt{5}}$
$\frac{3}{2}$	$-\frac{1}{2}$	$\frac{1}{2}$	$-\frac{1}{2\sqrt{5}}$	$-\frac{1}{2}$	$\frac{3}{2\sqrt{5}}$
$\frac{3}{2}$	$-\frac{3}{2}$	$\frac{1}{2}$	$-\frac{3}{2\sqrt{5}}$	$\frac{1}{2}$	$-\frac{1}{2\sqrt{5}}$

Table 2. The ratios of intensities of different magnetic sublevels of np hole states in spin-resolved spectra to that in spin-unresolved spectra for the geometry of experiment shown in figure 1 and linearly polarized light. $\boldsymbol{n}$ is the direction of the sample magnetization, and $\boldsymbol{e}$ is the light polarization vector.

		Intensity ratio			
j	m_j	$\boldsymbol{e}\perp\boldsymbol{n}, \boldsymbol{s}\|\boldsymbol{n}$	$\boldsymbol{e}\perp\boldsymbol{n}, \boldsymbol{s}\|-\boldsymbol{n}$	$\boldsymbol{e}\|\boldsymbol{n}, \boldsymbol{s}\|\boldsymbol{n}$	$\boldsymbol{e}\|\boldsymbol{n}, \boldsymbol{s}\|-\boldsymbol{n}$
$\frac{3}{2}$	$\frac{3}{2}$	1	0	0	0
$\frac{3}{2}$	$\frac{1}{2}$	0	1	1	0
$\frac{3}{2}$	$-\frac{1}{2}$	1	0	0	1
$\frac{3}{2}$	$-\frac{3}{2}$	0	1	0	0
$\frac{1}{2}$	$\frac{1}{2}$	0	1	1	0
$\frac{1}{2}$	$-\frac{1}{2}$	1	0	0	1

Consider now the same geometry of experiment but with light linearly polarized parallel to the magnetization direction $\boldsymbol{n}$ (s-polarized light; see figure 1). Then, from equation (7), one obtains

$$I_{1/2}(\boldsymbol{\kappa}, \boldsymbol{s}, \boldsymbol{n}) = \frac{\sigma(\omega)}{4\pi\sqrt{2}}(\rho^{\boldsymbol{n}}_{00} \pm \rho^{\boldsymbol{n}}_{10})(1 - \tfrac{1}{2}\beta) \tag{13}$$

$$I_{3/2}(\boldsymbol{\kappa}, \boldsymbol{s}, \boldsymbol{n}) = \frac{\sigma(\omega)}{4\pi}\left(\rho^{\boldsymbol{n}}_{00} - \rho^{\boldsymbol{n}}_{20} \pm \frac{1}{\sqrt{5}}\rho^{\boldsymbol{n}}_{10} \mp \frac{3}{\sqrt{5}}\rho^{\boldsymbol{n}}_{30}\right)(1 - \tfrac{1}{2}\beta) \tag{14}$$

where again the upper and lower signs refer to the cases when $\boldsymbol{s}\|\boldsymbol{n}$ and $\boldsymbol{s}\|-\boldsymbol{n}$. The relative contributions of each magnetic sublevel in this case are also given in table 2. Now only one of magnetic sublevels of the $n\mathrm{p}_{3/2}$ final state contributes to the spin-resolved photoelectron intensity, which is favourable for investigation of the energy positions of different magnetic sublevels. It is worthwhile stressing that the ratios in table 2 are independent of the angle θ.

Finally, if light is unpolarized while all other vectors are directed as before (see figure 1), the angular distributions become more complicated functions of the angle θ:

$$I_{1/2}(\boldsymbol{\kappa},\boldsymbol{s},\boldsymbol{n}) = \frac{\sigma(\omega)}{4\pi\sqrt{2}}\{\rho^n_{00}(1-\tfrac{1}{2}\beta)+(\rho^n_{00}\mp\rho^n_{10})[\tfrac{3}{4}\beta\cos^2\theta\pm\tfrac{1}{2}\eta^{1/2}\sin(2\theta)]\} \tag{15}$$

$$\begin{aligned} I_{3/2}(\boldsymbol{\kappa},\boldsymbol{s},\boldsymbol{n}) = \frac{\sigma(\omega)}{4\pi}\Bigg[&\left(\rho^n_{00}\pm\frac{3\sqrt{5}}{10}\rho^n_{10}-\tfrac{1}{4}\rho^n_{20}\mp\frac{3}{4\sqrt{5}}\rho^n_{30}\right)(1-2\beta+\tfrac{3}{2}\beta\sin^2\theta)\\ &+\tfrac{9}{4}big g(\rho^n_{00}\pm\frac{\sqrt{5}}{3}\rho^n_{10}\right)\beta\cos^2\theta\pm\left(\tfrac{1}{2}\rho^n_{00}\pm\frac{\sqrt{5}}{2}\rho^n_{10}+\rho^n_{20}\right)\eta^{3/2}\sin(2\theta)\Bigg] \end{aligned} \tag{16}$$

where the upper and lower signs refer again to the cases $(M\uparrow, s\uparrow)$ and $(M\uparrow, s\downarrow)$, respectively. To obtain the equations for the cases $(M\downarrow, s\downarrow)$ and $M\downarrow, s\uparrow)$, one should reverse the signs of the terms with $\sin(2\theta)$ in equations (15) and (16) for the cases $(M\uparrow, s\uparrow)$ and $(M\uparrow, s\downarrow)$, respectively. The ratios $I_j(\boldsymbol{\kappa},\boldsymbol{s},\boldsymbol{n})/I_j(\boldsymbol{\kappa},\boldsymbol{n})$ of the intensity of the different magnetic sublevels in the spin-resolved spectrum to that in spin-unresolved spectrum, which are now functions of the angle θ, are presented in table 3. They are less interesting in the sense that now all sublevels but one contribute simultaneously, so that the spin-resolved spectrum does not differ much from the spin-unresolved spectrum. Only in the limiting case when $\beta = 2$ are the ratios in table 3 the same as in table 2 in the case when $\boldsymbol{e}\perp\boldsymbol{n}$.

Table 3. The ratios of intensities of different magnetic sublevels in spin-resolved spectrum to that in spin-unresolved spectrum for np core levels. The geometry of experiment is shown in figure 1; light is unpolarized.

		Intensity ratio	
j	m_j	$\boldsymbol{s}\|\boldsymbol{n}$	$\boldsymbol{s}\|-\boldsymbol{n}$
$\frac{3}{2}$	$\frac{3}{2}$	1	0
$\frac{3}{2}$	$\frac{1}{2}$	$\frac{4-2\beta}{5-\beta-\frac{3}{2}\beta\sin^2\theta+2\eta^{3/2}\sin(2\theta)}$	$\frac{1+\beta-\frac{3}{2}\beta\sin^2\theta+2\eta^{3/2}\sin(2\theta)}{5-\beta-\frac{3}{2}\beta\sin^2\theta+2\eta^{3/2}\sin(2\theta)}$
$\frac{3}{2}$	$-\frac{1}{2}$	$\frac{1+\beta-\frac{3}{2}\beta\sin^2\theta-2\eta^{3/2}\sin(2\theta)}{5-\beta-\frac{3}{2}\beta\sin^2\theta-2\eta^{3/2}\sin(2\theta)}$	$\frac{4-2\beta}{5-\beta-\frac{3}{2}\beta\sin^2\theta-2\eta^{3/2}\sin(2\theta)}$
$\frac{3}{2}$	$-\frac{3}{2}$	0	1
$\frac{1}{2}$	$\frac{1}{2}$	$\frac{2-\beta}{4+\beta-3\beta\sin^2\theta-2\eta^{1/2}\sin(2\theta)}$	$\frac{2+2\beta-3\beta\sin^2\theta-2\eta^{1/2}\sin(2\theta)}{4+\beta-3\beta\sin^2\theta-2\eta^{1/2}\sin(2\theta)}$
$\frac{1}{2}$	$-\frac{1}{2}$	$\frac{2+2\beta-3\beta\sin^2\theta+2\eta^{1/2}\sin(2\theta)}{4+\beta-3\beta\sin^2\theta+2\eta^{1/2}\sin(2\theta)}$	$\frac{2-\beta}{4+\beta-3\beta\sin^2\theta+2\eta^{1/2}\sin(2\theta)}$

Consider now the absorption of circularly polarized light in the experiment geometry shown in figure 1 with magnetization along $\boldsymbol{n}'$. Suppose that light is left circularly polarized, i.e. the dipole operator in our laboratory frame is proportional to $Y_{11}(\vartheta,\varphi)$, and the photon spin $\boldsymbol{s}_\gamma$ is directed along the laboratory Z axis. The photoelectron spin polarization will

also be defined along the direction of sample magnetization. Then from equation (7) we find that

$$I_{3/2}(\boldsymbol{\kappa},\boldsymbol{s},\boldsymbol{n}) = \frac{\sigma}{4\pi}\left\{\left(1+\frac{\beta}{4}\right)\left(\rho_{00}^{n} \pm \frac{2}{\sqrt{5}}\rho_{10}^{n} + \tfrac{1}{2}\rho_{20}^{n} \pm \frac{3}{2\sqrt{5}}\rho_{30}^{n}\right) - \left(1+\frac{\beta}{4}-\tfrac{9}{4}W\right) \times\left(\pm\tfrac{1}{2}\rho_{00}^{n} + \frac{\sqrt{5}}{2}\rho_{10}^{n} \pm \rho_{20}^{n}\right)\cos\theta - \left[\tfrac{3}{4}\beta\rho_{00}^{n} \pm \frac{1}{2\sqrt{5}}(1+\tfrac{5}{2}\beta)\rho_{10}^{n} + \tfrac{27}{40}W\rho_{20}^{n} \pm \frac{9}{4\sqrt{5}}\rho_{30}^{n}\right]\sin^2\theta\right\} \tag{17}$$

$$I_{1/2}(\boldsymbol{\kappa},\boldsymbol{s},\boldsymbol{n}) = \frac{\sigma(\omega)}{4\pi\sqrt{2}}\left\{(\rho_{00}^{n} \mp \rho_{10}^{n})\left[1+\frac{\beta}{4} \pm \left(1+\frac{\beta}{4}-\tfrac{9}{4}W\right)\cos\theta\right] - \left[\tfrac{3}{4}\beta\rho_{00}^{n} \mp \left(1+\frac{\beta}{4}\right)\rho_{10}^{n}\right]\sin^2\theta\right\} \tag{18}$$

where the upper and lower signs refer to the cases when $\boldsymbol{s}\|\boldsymbol{n}'$ and $\boldsymbol{s}\|-\boldsymbol{n}'$, or $(M\uparrow, s\uparrow)$ and $(M\uparrow, s\downarrow)$,

$$W = \frac{d_d^2}{d_s^2 + d_d^2} \tag{19}$$

where d_d and d_s are the reduced dipole matrix elements [24]. The equations for $(M\downarrow, s\downarrow)$ and $(M\downarrow, s\uparrow)$ are obtained from the corresponding equations (17) and (18) for $(M\uparrow, s\uparrow)$ and $(M\uparrow, s\downarrow)$ by reversing the sign of the term with $\cos\theta$. For right circularly polarized light the same equations hold but with the reversed directions of both $\boldsymbol{n}'$ and $\boldsymbol{s}$.

4. Discussion

Since spin-resolved measurements are much more complicated than spin-unresolved measurements, it is worthwhile trying to understand what kind of new information can be extracted from them. In the case of ferromagnets it is important to investigate the magnetic splitting of core levels. Usual photoelectron spectroscopy could not resolve the magnetic sublevels since their widths are larger than the energy splittings [6, 7, 11]. As was shown above (see table 2), spin-resolved measurements in the geometry of figure 1 allow one to exclude the contributions of some magnetic sublevels and in this way to resolve the magnetic splitting of levels. In the case of s-polarized light, just one magnetic sublevel of the $n\mathrm{p}_{3/2}$ and $n\mathrm{p}_{1/2}$ subshells contributes. In the case of p-polarized light, every second magnetic sublevel contributes, which is also favourable for resolving the magnetic structure. With circularly polarized light, as follows from equations (17) and (18) provided that $\theta \neq 0$, all magnetic sublevels give a non-zero contribution, and only in the limit $\theta \to 0$ do they give the same qualitative result as linearly polarized light with $\boldsymbol{e} \perp \boldsymbol{n}$ (see table 2). In the case of unpolarized light, evidently, the picture is also less clear than with linearly polarized light (see table 3). So, for the geometry of experiment considered above, the analysis of photoelectron spin enables one to separate the contributions of different magnetic sublevels when linearly polarized light is used.

On the other hand, it was shown in [15] that four magnetic sublevels of the $n\mathrm{p}_{3/2}$ state can be resolved in MDAD measurements with s-polarized light even without spin detection of photoelectrons, but one could not resolve in this way the magnetic sublevels of the $n\mathrm{p}_{1/2}$ state. An advantage of MDAD arises from the fact that it is a difference between two angular distributions where many terms cancel out. One can also consider

differences between two spin-resolved angular distributions. Since there are four different combinations of the directions of vectors $\boldsymbol{s}$ and $\boldsymbol{n}$, one can define six differences between angular distributions. Some of them are rather simple, which can help one to analyse experimental spectra and to extract the theoretical parameters from the measured data; the others are not simple and hardly help in the interpretation of spectra. Consider as an example two differences between the spectra given by equation (12) for p-polarized light:

$$I_{3/2}(M\uparrow, s\uparrow) - I_{3/2}(M\downarrow, s\downarrow) = \frac{\sigma(\omega)}{2\pi}(\rho^n_{00} + \sqrt{5}\rho^n_{10} + 2\rho^n_{20})\eta^{3/2}\sin(2\theta) \tag{20}$$

$$I_{3/2}(M\uparrow, s\uparrow) - I_{3/2}(M\uparrow, s\downarrow) = \frac{\sigma(\omega)}{2\pi}\left[\frac{2}{\sqrt{5}}(\rho^n_{10} + \tfrac{3}{4}\rho^n_{30})(1 + \beta - \tfrac{3}{2}\beta\sin^2\theta) + (\rho^n_{00} + 2\rho^n_{20})\eta^{3/2}\sin(2\theta)\right]. \tag{21}$$

Equation (20) is simpler than (12), and the corresponding difference can be used to extract the parameter $\eta^{3/2}$ from the experiment. Using table 1, one can easily find that the sum of state multipoles, $\rho^n_{00} + \sqrt{5}\rho^n_{10} + 2\rho^n_{20}$, in equation (20) is equal to 3 and -1 for the $m_j = \frac{3}{2}$ and $m_j = -\frac{1}{2}$ magnetic sublevels, respectively, and to zero in the two other sublevels. The difference between the corresponding experimental curves presented in the lower part of figure 3 in [4] show qualitatively just this behaviour. Equation (20) gives an example of the terms which were excluded from the model consideration of [17], since the spin polarization parameter η^j is just the interference term between the $l+1$ and $l-1$ continuum channels neglected in [17]. Equation (21) contains the same terms as (12) but with different linear combinations of state multipoles. As a result, the difference (21) is non-zero in all magnetic sublevels, and therefore its determination could not be used so easily for qualitative analysis of the data. The disadvantage in determining the differences is connected with much larger error bars in them.

Determination of differences is more helpful when the initial expressions are complicated, as in particular in the cases of circularly polarized and unpolarized light considered above. For example, in the case of unpolarized light, one can obtain from equations (15) and (16)

$$I_{1/2}(M\uparrow, s\uparrow) - I_{1/2}(M\downarrow, s\downarrow) = \frac{\sigma(\omega)}{4\pi\sqrt{2}}(\rho^n_{00} - \rho^n_{10})\eta^{1/2}\sin(2\theta) \tag{22}$$

$$I_{3/2}(M\uparrow, s\uparrow) - I_{3/2}(M\downarrow, s\downarrow) = \frac{\sigma(\omega)}{4\pi}(\rho^n_{00} + \sqrt{5}\rho^n_{10} + 2\rho^n_{20})\eta^{3/2}\sin(2\theta). \tag{23}$$

These differences have non-zero values for the magnetic sublevels with $m_j = \frac{3}{2}$ and $m_j = -\frac{1}{2}$ and are equal to zero for other sublevels. Therefore their determination can help in the interpretation of experimental spectra, provided that the error bars are reasonably small. Qualitatively the same answer follows from equations (17) and (18) for the analogous differences in the case of circularly polarized light.

One can define not only the differences but also the sums of two spectra [29]. From equation (12) for linearly polarized light it follows, for example, that

$$I_{3/2}(M\uparrow, s\uparrow) + I_{3/2}(M\downarrow, s\downarrow) = \frac{\sigma(\omega)}{2\pi}\left(\rho^n_{00} + \tfrac{1}{2}\rho^n_{20} + \frac{2}{\sqrt{5}}\rho^n_{10} + \frac{3}{2\sqrt{5}}\rho^n_{30}\right)(1 + \beta - \tfrac{3}{2}\beta\sin^2\theta) \tag{24}$$

which is again simpler than (12) and contains only the asymmetry parameter β. Since the error bars in the sum are much smaller than in the difference, their determination can be more successfully used to extract the values of theoretical parameters from experiment.

Using the equations given above, one can easily find the other differences or sums of the intensities and choose the values which are most appropriate for the analysis of the data obtained for a particular geometry of experiment. In the cases of circularly polarized and unpolarized light the determination of these differences will simplify the analysis of spectra, while for linearly polarized light the spectra themselves are relatively simple so that one can analyse them without defining the differences.

5. Conclusions

We have derived the general equations describing the angle- and spin-resolved photoemission from core levels of ferromagnets in the atomic model. They have been applied to the analysis of photoemission normal to the surface from np core levels. We showed that, in the case of linearly polarized light, one can reach the clearest separation of different magnetic sublevels because, for the given directions of magnetization and spin, only some of magnetic sublevels contribute to the photoelectron spectra. It gives a rather unique possibility to resolve the magnetic sublevels the widths of which are larger than their energy separation. In the cases of circularly polarized and unpolarized light, one could not reach such good separation of magnetic sublevels for the experiment geometries considered above. Therefore synchrotron radiation is particularly suitable for this kind of spin-resolved experiment.

In some cases it can be helpful to analyse the differences of two spin-resolved spectra which have simpler structure than the spectra themselves. In particular, it can be helpful when unpolarized light has been used to obtain spin-resolved spectra. These differences can be as simple as the spectra obtained with linearly polarized light, but the error bars in the differences are much larger, so that their investigation is not always feasible.

It is important that the relative intensities of different magnetic sublevels in the atomic model are independent of the angle of incidence of photons and their energy; therefore one does not need to perform any calculation in order to analyse qualitatively the experimental spectrum. It is sufficient to simulate the spin-unresolved spectrum by the Lorentzians with amplitudes obtained from the fit to the experimental spectrum, as has been done in [7], and then to multiply the intensities by the coefficients given in table 2 in order to obtain the spin-resolved spectrum. The first application of the atomic model to the analysis of experimental spectra, both spin unresolved [7, 15] and spin resolved [7, 29], showed that it correctly describes the qualitative features observed in the experiments.

We have studied in detail the particular cases of photoemission from np core levels because they have been investigated experimentally, and because they represent the simplest example. The general equations (7) and (8) can be applied also to nd and nf core levels, but the analysis of results will be more complicated because more state multipoles characterizing the polarization of the hole state will contribute simultaneously. In principle, the atomic model can be applied also to photoemission from valence bands, if one can describe the polarization of initial state by state multipoles.

Acknowledgments

The authors acknowledge the financial support of the Russian Fund for Fundamental Research (grant 93-02-2579). NAC would like to express his gratitude to the Alexander von

Humboldt-Stiftung for the research award, and to the Bielefeld University for the hospitality extended to him during his stay.

References

[1] Baumgarten L, Schneider C M, Petersen H, Schäfers F and Kirschner J 1990 *Phys. Rev. Lett.* **65** 492
[2] Schneider C M, Venus D and Kirschner J 1992 *Phys. Rev.* B **45** 5041
[3] Bansmann J, Westphal C, Getzlaff M, Fegel F and Schönhense G 1992 *J. Magn. Magn. Mater*. **104–7** 1691
[4] Roth Ch, Hillebrecht F U, Rose H B and Kisker E 1993 *Phys. Rev. Lett.* **70** 3479
[5] Roth Ch, Rose H B, Hillebrecht F U and Kisker E 1993 *Solid State Commun.* **86** 647
[6] Sirotti F and Rossi G 1994 *Phys. Rev*. B **49** 15 682
[7] Rossi G, Sirotti F, Cherepkov N A, Combet Farnoux F and Panaccione G 1994 *Solid State Commun.* **90** 557
[8] Hillebrecht F U and Herberg W-D 1994 *Z. Phys.* B **93** 299
[9] Getzlaff M, Ostertag Ch, Fecher G H, Cherepkov N A and Schönhense G 1994 *Phys. Rev. Lett.* **73** 3030
[10] Carbone C and Kisker F 1988 *Solid State Commun.* **65** 1107
[11] Ebert H, Baumgarten L, Schneider C M and Kirschner J 1991 *Phys. Rev.* B **44** 4406
[12] Scheunemann T, Halilov S V, Henk J and Feder R 1994 *Solid State Commun.* **91** 487
[13] Venus D 1994 *Phys. Rev.* B **49** 8821
[14] Thole B T and van der Laan G 1994 *Phys. Rev.* B **49** 9613
[15] Cherepkov N A 1994 *Phys. Rev.* B **50** 13 813
[16] Roth Ch, Hillebrecht F U, Park W G, Rose H B and Kisker E 1994 *Phys. Rev. Lett.* **73** 1963
[17] Huang D-J, Riffe D M and Erskine J L 1995 *Phys. Rev.* B **51** 15 170
[18] Kakehashi Y 1985 *Phys. Rev.* B **32** 1607
[19] Cherepkov N A 1974 *Sov. Phys.–JETP* **38** 463
[20] Rose M E 1957 *Elementary Theory of Angular Momentum* (New York: Wiley)
[21] Jacobs V L 1972 *J. Phys. B: At. Mol. Phys.* **5** 2257
[22] Kabachnik N M and Sazhina I P 1976 *J. Phys. B: At. Mol. Phys.* **9** 1681
[23] Klar H and Kleinpoppen H 1982 *J. Phys. B: At. Mol. Phys.* **15** 933
[24] Cherepkov N A 1983 *Adv. At. Mol. Phys.* **19** 395
[25] Blum K 1981 *Density Matrix Theory and Applications* (New York: Plenum)
[26] Kuznetsov V V 1989 *PhD Thesis* St Petersburg State University
[27] Cherepkov N A, Kuznetsov V V and Verbitskii V A 1995 *J. Phys. B: At. Mol. Opt. Phys.* **28** 1221
[28] van der Laan G 1995 *Phys. Rev.* B **51** 240
[29] Hillebrecht F U, Rose H B, Roth Ch, Park W G, Kisker E and Cherepkov N A 1996 *Phys. Rev.* B at press